Naval Research Laboratory

Washington, DC 20375-5320

Initial Parameter Estimation for Inverse Thermal Analysis of Ti-6Al-4V Deep Penetration Welds

S.G. LAMBRAKOS
L. HUANG

Center for Computational Materials Science
Materials Science and Technology Division

A. SHABAEV

George Mason University
Fairfax, Virginia

May 16, 2014

REPORT DOCUMENTATION PAGE

Public reporting burden for this collection of information is estimated to average 1 hour per response, including the time for reviewing instructions, searching existing data sources, gathering and maintaining the data needed, and completing and reviewing this collection of information. Send comments regarding this burden estimate or any other aspect of this collection of information, including suggestions for reducing this burden to Department of Defense, Washington Headquarters Services, Directorate for Information Operations and Reports (0704-0188), 1215 Jefferson Davis Highway, Suite 1204, Arlington, VA 22202-4302. Respondents should be aware that notwithstanding any other provision of law, no person shall be subject to any penalty for failing to comply with a collection of information if it does not display a currently valid OMB control number. **PLEASE DO NOT RETURN YOUR FORM TO THE ABOVE ADDRESS.**

1. REPORT DATE (DD-MM-YYYY) 16-05-2014	2. REPORT TYPE NRL Memorandum Report	3. DATES COVERED (From - To) October 1, 2013 – March 1, 2014

4. TITLE AND SUBTITLE	5a. CONTRACT NUMBER
Initial Parameter Estimation for Inverse Thermal Analysis of Ti-6Al-4V Deep Penetration Welds	5b. GRANT NUMBER
	5c. PROGRAM ELEMENT NUMBER
6. AUTHOR(S)	5d. PROJECT NUMBER
S.G. Lambrakos, L. Huang, and A. Shabaev[1]	5e. TASK NUMBER
	5f. WORK UNIT NUMBER 63-2509-R4

7. PERFORMING ORGANIZATION NAME(S) AND ADDRESS(ES)	8. PERFORMING ORGANIZATION REPORT NUMBER
Naval Research Laboratory, Code 6394 4555 Overlook Avenue, SW Washington, DC 20375-5320	NRL/MR/6390--14-9542

9. SPONSORING / MONITORING AGENCY NAME(S) AND ADDRESS(ES)	10. SPONSOR / MONITOR'S ACRONYM(S)
Office of Naval Research One Liberty Center 875 North Randolph Street, Suite 1425 Arlington, VA 22203-1995	ONR
	11. SPONSOR / MONITOR'S REPORT NUMBER(S)

12. DISTRIBUTION / AVAILABILITY STATEMENT

Approved for public release; distribution is unlimited.

13. SUPPLEMENTARY NOTES

[1]George Mason University, Department of Computation and Data Sciences, Fairfax, VA 22030

14. ABSTRACT

Case study inverse thermal analyses of Ti-6Al-4V deep penetration welds are presented. These analyses employ a methodology that is in terms of analytical basis functions for inverse thermal analysis of steady state energy deposition in plate structures. The results of the case studies provide parametric representations of weld temperature histories that can be adopted as input data to various types of computational procedures, such as those for prediction of solid-state phase transformations. In addition, these temperature histories can be used to construct parametric-function representations for inverse thermal analysis of welds corresponding to other process parameters or welding processes whose process conditions are within similar regimes. This study also discusses specific aspects of the inverse-analysis methodology relevant to further development of algorithms for its application in practice.

15. SUBJECT TERMS

Inverse-analysis methodology	Deep penetration welds
Inverse thermal analysis	Weld temperature histories

16. SECURITY CLASSIFICATION OF:			17. LIMITATION OF ABSTRACT	18. NUMBER OF PAGES	19a. NAME OF RESPONSIBLE PERSON Samuel G. Lambrakos
a. REPORT Unclassified Unlimited	b. ABSTRACT Unclassified Unlimited	c. THIS PAGE Unclassified Unlimited	Unclassified Unlimited	36	19b. TELEPHONE NUMBER (include area code) (202) 767-2601

CONTENTS

Introduction

Case study inverse thermal analyses of Ti-6Al-4V deep penetration welds are presented. These analyses provide a parameterization of temperature histories for prediction of properties within the Heat Affected Zone (HAZ) of welds for the regime considered. These analyses employ a procedure that is in terms of numerical-analytical basis functions for steady state energy deposition in plate structures. The formal structure of the numerical methodology underlying this procedure follows from a specific definition of the inverse heat transfer problem, which is well posed for inverse analysis of heat deposition processes. This definition is based on the assumption of the availability of information concerning spatially distributed boundary and constraint values. The present study represents another extension of an inverse thermal analysis procedure applied in previous studies. This extension provides for the incluion of constraint conditions associated with both solidification and phase transformation boundaries. For the present study, which considers Ti-6Al-4V deep penetration welds, the phase transformation boundary adopted for temperature-field constraint conditions is that of the α to β phase transformation.

The results of the case study presented provide parametric representations of weld temperature histories that can be adopted as input data to various types of computational procedures, such as those for prediction of solid-state phase transformations and associated software implementations. In addition, these weld temperature histories can be used for construction of numerical basis functions that can be adopted for inverse analysis of welds corresponding to other process parameters or welding processes whose process conditions are within similar regimes. The construction of temperature fields according to spatially and temporally distributed constraint conditions using linear combinations of optimal basis functions represents a highly convenient approach to inverse analysis of energy deposition processes. Basis functions can be terms of function representations that are analytical, numerical and numerical-analytical, and these function representations in linear combination.

The rigorous mathematical foundation of the inverse analysis method used for calculation of temperature histories in this study is that of least-squares parameter optimization [1-4]. The elegance of the formalism underlying the inverse analysis methodology applied in this study may convey the notion of approximation or oversimplification in terms of model representation relative to models formulated using finite element, finite volume and finite difference methods, which are structured for first-principles based simulation. This is indeed not the case in that a significant aspect of least-squares parameter optimization is choice of a sufficiently complete set of basis functions. A sufficiently complete set of basis functions implies that all possible modes of a given heat deposition process can be represented by a linear combination of these functions. The use of Green's functions corresponding to various types of fundamental solutions to the heat conduction equation establishes that the basis functions used for inverse heat deposition analysis are equipped with trend characteristics associated with diffusion, advection in the weld melt pool and relative motion of the workpiece. In addition, the formal structure of least-squares based methods establishes that all forms of experimental information can be embedded directly as constraints conditions on the parameters (or coefficients) to be optimized.

Models that are formulated in terms of basic theory are difficult to apply for quantitative weld analysis in that most material properties needed for this type of modeling are not available. The inverse modeling approach compensates for this lack of information. For example, one goal of models formulated in terms of basic theory, for the case of deep-penetration welding, is simulation of the coupling of keyhole formation, melting, fluid flow in the weld melt pool and

heat transfer from the solidification boundary into the heat effected zone (HAZ). It is important to note that with respect to practical analysis the purpose of modeling these influences, in particular, would be generation of the solidification boundary, the surface from which heat is transferred into the HAZ, the region of most probable weld failure. The inverse analysis approach adopts information concerning the solidification boundary as "model input" and thus compensates for the lack information associated with underlying physical mechanisms. Accordingly, the information content of the inverse analysis methodology applied in the present study, in principle, exceeds that of a direct problem approach for calculation of the solidification boundary.

Models that are formulated in terms of basic theory, whose structure is for the inclusion of underlying physical mechanisms are inherently complex and thus require large-scale calculations, which in many cases are at the limit of computational capabilities. As a result, the computational cost of direct modeling is prohibitive with respect to calculation of temperature histories, which is the focus the present study. It is important to note, however, that true insight into the nature of underlying mechanisms can only be achieved using direct modeling, which in turn establishes what are reasonable parametric representations for inverse modeling, e.g., the Green's functions used in the present study.

Next, although the mathematical foundation of inverse modeling is both elegantly formulated and well defined in terms of least-squares parameter optimization, it should be appreciated that fitting inverse model parameters does in itself pose a difficult problem. Accordingly, further investigation should be applied to the development of more efficient algorithms for parameter optimization with respect to a wide range of different types measurements associated with welding processes.

Finally, it must be noted that a fundamental aspect of inverse analysis is that there does not exist a unique model representation for purposes of inversion. In practice, inverse models are typically structured for the specific quantity or parameter to be determined, including material properties. For example, reference [5] presents an inverse analysis using numerical simulations related to direct modeling for the determination of unknown variables. Reference [6] addresses the mathematical property that, because of the non-uniqueness of inverse models, every inverse problem is to be associated with an "inverse model space" rather than a unique inverse model. The inverse method presented in this manuscript is for the purpose of calculating temperature histories, and as indicated above has various advantages for this specific purpose.

The organization of the subject areas presented here are as follows. First, a brief description of the general procedure for inverse analysis of heat deposition processes is presented. Second, results of inverse thermal analyses of Ti-6Al-4V deep penetration welds (laser and electron beam) are presented. These results provide a quantitative parametric representation of temperature histories for these welds and for any welds associated with similar welding process conditions. Third, a discussion is presented concerning aspects of the inverse analysis methodology that are relevant to its further development. Finally, a conclusion is given.

Inverse Analysis Procedure

Following the inverse analysis approach [7-17], a parametric representation based on a physical model provides a means for the inclusion of information concerning the physical characteristics of a given energy deposition process. It follows then that for heat deposition processes involving the deposition of heat within a bounded region of finite volume, consistent parametric representations of the temperature field are given by

$$T(\hat{x},t) = T_A + \sum_{k=1}^{N_k} w_k T_k(\hat{x},\hat{x}_k,\kappa,t) \qquad \text{(Eq 1a)}$$

and
$$T(\hat{x}_n^c, t_n^c) = T_n^c \qquad \text{(Eq 1b)}$$

where $T_k(\hat{x},\hat{x}_k,\kappa,t)$ and w_k represent an effectively complete set of basis functions and their weighting coefficients, respectively, for representation of the temperature field within a region bounded by specified inner and outer surfaces S_i and S_o, respectively. The quantity T_A is the ambient temperature of the workpiece and the locations $\hat{x}_n^c$ and temperature values T_n^c specify constraint conditions on the temperature field. The functions $T_k(\hat{x},\hat{x}_k,\kappa,t)$ represent an optimal basis set of functions for given sets of boundary conditions and material properties. The quantities $\hat{x}_k = (x_k, y_k, z_k)$, $k=1,...,N_k$, are the locations of the elemental source or boundary elements. The sum defined by Eq.(1a) can for certain systems specify numerical integration over discrete elements of a distribution of sources or boundary elements. Selection of an optimal set of basis functions is based on a consideration of the characteristic model and data spaces [6] of heat deposition processes and subsequently isolating those regions of the model space corresponding to parameterizations that are both physically consistent and sufficiently general in terms of their mathematical representation and mapping from data to model space. Although heat deposition processes may be characterized by complex coupling between the heat source and workpiece, as well as complex geometries associated with either the workpiece or deposition process, in terms of inverse analysis the general functional forms of the temperature fields associated with all such processes are within a restricted class of functions, i.e., optimal sets of basis functions. Accordingly, a sufficiently optimal set of basis functions can be constructed using numerically-integrated analytic solutions to heat conduction equation for a finite set of boundary conditions [18]. The present study utilizes basis functions that are numerical-analytical solutions to the heat conduction equation. Parameterizations that are based on this set of functions are both sufficiently general and convenient relative to optimization.

The formal procedure underlying the inverse method considered here entails the adjustment of the temperature field defined over the entire spatial region of the sample volume at a given time t. This approach defines an optimization procedure where the temperature field spanning the spatial region of the sample volume is adopted as the quantity to be optimized. The constraint conditions are imposed on the temperature field spanning the bounded spatial domain of the workpiece by minimization of the value of the objective functions defined by

$$Z_T = \sum_{n=1}^{N} w_n \left(T(\hat{x}_n^c, t_n^c) - T_n^c \right)^2 \qquad \text{(Eq 2)}$$

where T_n^c is the target temperature for position $\hat{x}_n^c = (x_n^c, y_n^c, z_n^c)$. The quantities w_n ($n=1,...,N$) are weight coefficients that specify relative levels of influence associated with constraint conditions T_n^c.

The input of information into the inverse model defined by Eqs. (1) and (2), i.e., the mapping from data to model space, is effected by: the assignment of individual constraint values to the quantities T_n^c; the form of the basis functions adopted for parametric representation; and specifying the shapes of the inner and outer boundaries, S_i and S_o, respectively, which bound the

temperature field within a specified region of the workpiece. The constraint conditions and basis functions, i.e., $T(\hat{x}_n^c, t_n^c) = T_n^c$ and $T_k(\hat{x}, \hat{x}_k, \kappa, t)$, respectively, provide for the inclusion of information that can be obtained from both laboratory and numerical experiments.

Within the context of the numerical method presented, a set of basis functions is considered effectively complete if these functions provided reasonably optimal fitting to boundary and constraint conditions. Before proceeding it is significant to note that in principle the set of basis functions adopted by Eq.(1) can be defined in terms of either analytical or numerical function representations. The numerical method that is developed here employs both analytical and numerical function representations of basis functions, which are to be adopted for the calculation of temperature fields within bounded domains for which constraint conditions are specified. Finally, the interrelation between analytical and numerical basis function representations is an important aspect of the numerical method applied in this analysis, which underlies it flexibility for convenient inverse analysis.

It follows then that a consistent representation Eq.(1) of the temperature field for heat deposition within structures characterized by a finite thickness, in terms of analytical basis functions, i.e., analytical solutions to the heat conduction equation [18] adopted as Green's functions, is

$$T(\hat{x}, t) = T_A + \sum_{k=1}^{N_k} \sum_{n=1}^{N_t} C(\hat{x}_k) G(\hat{x}, \hat{x}_k, \kappa, n\Delta t, V) \qquad \text{(Eq 3a)}$$

and

$$T(\hat{x}_n^c, t_n^c) = T_n^c, \qquad \text{(Eq 3b)}$$

where

$$G(\hat{x}, \hat{x}_k, t, \kappa, V) = \frac{1}{t} \exp\left[-\frac{(x - x_k - Vt)^2 + (y - y_k)^2}{4\kappa t}\right]$$
$$\times \left\{1 + 2\sum_{m=1}^{\infty} \exp\left[-\frac{\kappa m^2 \pi^2 t}{l^2}\right] \cos\left[\frac{m\pi z}{l}\right] \cos\left[\frac{m\pi z_k}{l}\right]\right\}, \qquad \text{(Eq 4)}$$

and

$$C(\hat{x}) = \sum_{k=1}^{N_k} Q(\hat{x}_k) \delta(\hat{x} - \hat{x}_k). \qquad \text{(Eq 5)}$$

where $Q(\hat{x}_k)$ is the value of the discrete source function at location $\hat{x}_k$. The quantities κ, V and l are the thermal diffusivity, welding speed and plate thickness, respectively. The procedure for inverse analysis defined by Eqs.(2)-(5) entails adjustment of the parameters $C(\hat{x}_k)$, $\hat{x}_k$ and Δt defined over the entire spatial region of the workpiece.

It should be noted that the inverse analysis methodology defined by Eq.(2) through (5) is based on a parametric numerical-analytical model, which combines numerical integration with optimization of linear combinations of analytical Greens functions. In particular, Eq.(3a) defines a discrete numerical integration over time, where the time step Δt is specified according to the average energy deposited during the time Δt, for transition of the temperature field to steady state. Further, for constrained least-squares parameter optimization of the linear combination Eq.(3a), the analytical Green's functions are adopted as basis functions, and should not be misinterpreted as being associated with any form of direct model representation.

Further, it should be noted that the formulation of the inverse analysis methodology defined by Eq.(2) through (5) is equipped with a mathematical structure in terms of Green's functions and adjustable parameters, which satisfies all boundary conditions associated with welding of plate structures. This follows first from Eq.(4), which includes as a factor the Green's function, in terms of a Fourier series representation, for two parallel boundary surfaces having zero diffusion gradient, and second from Eq.(3b), which adopts the constraint conditions $T(\hat{x}_n^c, t_n^c) = T_M$ and T_{TB}, where T_M and T_{TB} are the melt temperature (at the solidification boundary) and start temperature for transformation (approximately at the transformation boundary), respectively.

Case Study Analyses of Ti-6Al-4V Deep Penetration Welds

The procedure for construction of numerical basis functions adopted in this case study entails calculation of the steady state temperature field for a specified range of sizes and shapes of the inner surface boundary S_i defined by the solidification and transformation boundaries for a range of welding process parameters. For this system, the parameter values assumed are $\kappa = 1.07$ x 10^{-5} m^{2}s^{-1}, $T_M = 1605$ ^{o}C, $T_{TB} = 885$ ^{o}C and the values of l defined in Eqn. (3) are given in the figures below. The upstream boundary constraints on the temperature field, $T_c = T_M$ and T_{TB} for (y_c, z_c), defined in Eqn. (3), are given in Tables 1 and 2, respectively. These constraints are such that the calculated temperature field satisfies the conditions $T(\hat{x}, t) < T_M$ and $T(\hat{x}, t) < T_{TB}$. The transformation temperature T_{TB} was given the value of 885 ^{o}C, which is approximately the start temperature of the α to β phase transformation for Ti. As discussed further below, reasonable estimates of values for κ, T_M and T_{TB} are sufficient for the present analysis. Given in Tables 3 through 8 are values of the discrete source function that have been calculated according to the constraint conditions and weld process parameters given in Table 1. The relative location of each discrete source is specified according to Fig.1. Given in Tables 9 through 14 are values of the discrete source function that have been calculated according to the constraint conditions and weld process parameters given in Table 2. Again, the relative location of each discrete source is specified according to Fig.1. Shown in Figs. 2 through 31 are experimentally measured transverse weld cross sections of solidification and transformation boundaries (see references [19] and [20]), and different planar slices of the steady state temperature field that have been calculated according to the constraint conditions given in Tables 1 and 2. Referring to the planar slices of the calculated temperature fields, it can be seen that all boundary conditions are satisfied, namely the condition $T(\hat{x}, t) = T_M$ and $T(\hat{x}, t) = T_{TB}$ at the solidification and transformation boundaries, respectively, and $\nabla T \cdot \hat{n} = 0$ at surface boundaries, where $\hat{n}$ is normal to the surface.

Discussion

The general procedure for inverse thermal analysis of welds as described in this study includes interpolation between constrained isothermal boundaires, e.g., T_{TB} and T_M. A specific procedure for interpolation, however, has not been considered. For the present study, the close proximity of the isotherms considered (see Figs. 6, 11, 16, 21, 26 and 31) implies that relatively simple interpolation procedures can be applied, e.g., linear one-dimesional interpolation. In general, however, this should not be the case. For example, the inclusion of constrained isothermal surfaces associated thermocouple measurements may require three-dimensional

interpolation procedures. Accordingly, further investigation is needed to determine a general and optimal procedure for interpolation between constrained isothermal surfaces in three dimensions.

An important aspect of the inverse thermal analysis methodology applied here is that only a reasonable estimate of the diffusivity κ is needed. In particular, the quantity $\kappa\Delta t$ assumes the role of an adjustable parameter, in combination with the source values C_k, for generation of isothermal surfaces. The embedding of constrained isothermal surfaces within the calculated temperature field, which are based on experimental measurements, in principle, compensates for errors due to estimated values of the diffusivity function, which are in fact a function of temperature. This follows in that two or more embedded isothermal surfaces, which are sufficiently distributed volumetrically, represent implicitly the dependence of diffusivity on temperature. Accordingly, for the purpose of considering more accurately the temperature dependence of the thermal diffusivity, the procedure of embedding constrained isothermal surfaces can be extended to include more than two surfaces. This extension, however, as expected, increases the complexity of the procedure with respect to parameter optimization. Thus, the follwing must be emphasized.

Although the mathematical foundation of the inverse thermal analysis methodology presented is both elegantly formulated and well defined in terms of least-squares parameter optimization, it should be appreciated that fitting inverse model parameters does in itself pose a difficult problem. The continuing evolution of this methodology to include more, as well as different types of constraint conditions, based on experimental measurements, poses the problem of multi-parameter optimization. Accordingly, further investigation will be needed for development of more efficient algorithms for parameter optimization with respect to a wide range of different types measurements associated with welding processes.

It is emphasized that the results of this study are "initial parameter estimations for inverse thermal analysis of Ti-6Al-4V deep penetration welds." These estimates provide a starting point for further parameter optimization with respect to additional information, which would include both experimental measurements and results of numerical simulations employing detailed physical model representations. Accordingly, these parameter estimates are based on approximate values of the thermal diffusivity, solidus temperature T_M and start temperature T_{TB} of the α to β phase transformation in Ti-6Al-4V. The level of approximation assumed for estimated parameter values is consistent with the fact that exact locations of solidification and α to β transformation boundaries are difficult to determine experimentally [19, 20].

Conclusion

This report describes an inverse thermal analysis of Ti-6Al-4V deep penetration welds using multiple constraint conditions, which demonstartes the extension an inverse thermal analysis procedure applied in previous studies. The weld temperature histories obtained by this inverse analysis could in practice be used to predict not only solid-state phase transitions, but time and temperature within localized spatial regions associated with the evolution of plastic and elastic strains, resulting in distortion and residual stresses. The inverse analysis presented here concerns construction of a temperature field $T(\hat{x}, t, \kappa, V, S_M, S_{TB}, l)$, where it is assumed that the quantities κ, V, S_M, S_{TB} and l are known, and that $T(\hat{x}) = T_M$ and T_{TB} for all $\hat{x}$ on S_M and S_{TB}, respectively. As emphasized in previous studies, there are quantities other than the solidification boundary that are experimentally observable. In particular, the temperature fields extending over the top and bottom surfaces of the workpiece represent conveniently available data to be used for

inverse analysis. It is typical for the measurement of temperature histories at surfaces of workpieces to use thermocouples. In the case of relatively large welding speeds, the use of thermocouple measurements may require an additional adjustable parameter associated with thermocouple time delay.

Acknowledgment

References

1. R. W. Farebrother, Linear Least Square Computations, Marcel Dekker, New York, 1988.
2. Y. B. Bard, Nonlinear Parameter Estimation, Academic Press, New York. 1974.
3. K. Levenberg, "A Method for the Solution of Certain Non-linear Problems in Least-Squares", Quart. Appl. Math, 2, 164-168, 1944.
4. D. W. Marquardt, "An Algorithm for Least Squares Estimation of Nonlinear Parameters", J. Soc. Ind. Appl. Moth, II, 431-441, 1963.
5. S. Mishra and T. DebRoy, Tailoring Gas Tungsten Arc Weld Geometry using a Genetic Algorithm and a Neural Network Trained with Convective Heat Flow Calculations, Materials Science and Engineering A, 2007, vol. 454–455, pp. 477–486.
6. A. Tarantola: Inverse Problem Theory and Methods for Model Parameter Estimation, SIAM, Philadelphia, PA, 2005.
7. M. N. Ozisik and H. R. B. Orlande: Inverse Heat Transfer, Fundamentals and Applications, Taylor and Francis, New York, 2000.
8. K. Kurpisz and A. J. Nowak: Inverse Thermal Problems, Computational Mechanics Publications, Boston, USA, 1995.
9. O. M. Alifanov, Inverse Heat Transfer Problems. Springer, Berlin, 1994.
10. J. V. Beck, B. Blackwell, C. R. St. Clair, Inverse Heat Conduction: Ill-Posed Problems, Wiley Interscience, New York, 1985.
11. J. V. Beck, "Inverse Problems in Heat Transfer with Application to Solidification and Welding," Modeling of Casting, Welding and Advanced Solidification Processes V, M. Rappaz, M.R. Ozgu and K. W. Mahin eds., The Minerals, Metals and Materials Society, 1991, pp. 427-437.
12. J. V. Beck, "Inverse Problems in Heat Transfer," Mathematics of Heat Transfer, G.E. Tupholme and A.S. Wood eds., Clarendon Press, (1998), pp. 13-24.
13. S. G. Lambrakos, A. D. Zervaki, G. N. Haidemenopoulos and V. Stergiou, Basis Functions and Parameterizations for Inverse Analysis of Welding Processes, 'Mathematical Modelling of Weld Phenomena,' Volume 9, 793, Published by Verlag der Technischen Universite Graz, Austria (2011).
14. A. D. Zervaki, G. N. Haidemenopoulos and S. G. Lambrakos, Analysis of Heat Affected Zone using Direct and Inverse Modelling in 6XXX Aluminum Alloys,' Mathematical Modelling of Weld Phenomena,' Volume 8, 907, Published by Verlag der Technischen Universite Graz, Austria (2007).
15. S. G. Lambrakos and S. G. Michopoulos, Algorithms for Inverse Analysis of Heat Deposition Processes, 'Mathematical Modelling of Weld Phenomena,' Volume 8, 847, Published by Verlag der Technischen Universite Graz, Austria (2007).

16. S. G. Lambrakos and J. O. Milewski, Analysis of Welding and Heat Deposition Processes using an Inverse-Problem Approach, Mathematical Modelling of Weld Phenomena, **7**, 1025, Publishied by Verlag der Technischen Universite Graz, Austria 2005, pp. 1025-1055.
17. J. Xie, and J. Zou, Numerical Reconstruction of Heat Fluxes, SIAM J. Numer. Anal. 43, 4, 1504-1535, 2005.
18. H. S. Carslaw and J. C. Jaegar: Conduction of Heat in Solids, Clarendon Press, Oxford, 2nd ed, 374, 1959.
19. R. Rai, J.W. Elmer, T.A. Palmer, T. DebRoy, Heat Transfer and Fluid Flow During Keyhole Mode Laser Welding of Tantalum, Ti-6Al-4V, 304L Stainless Steel and Vanadium, J. Phys. D: Appl. Phys. 40, 5753-5766, 2007.
20. R. Rai, P. Burgardt, J. O. Milewski, T. J. Lienert, T. DebRoy, Heat Transfer and Fluid Flow During Electron Beam Welding of 21Cr-6Ni-9Mn Steel and Ti-6Al-4V Alloy, J. Phys. D: Appl. Phys. 42, 025503, 2009.
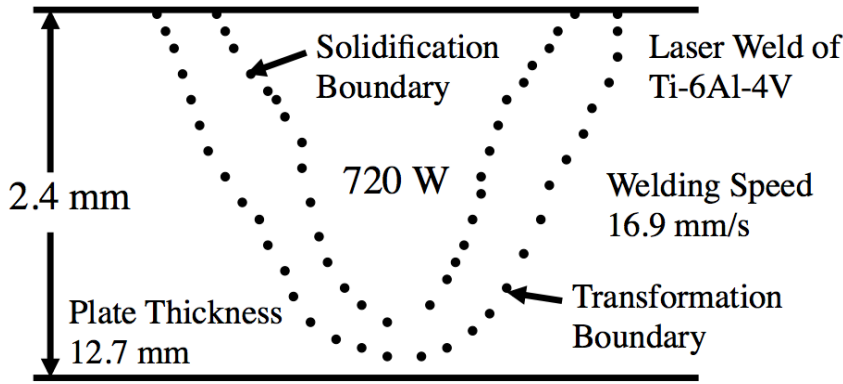
Figures
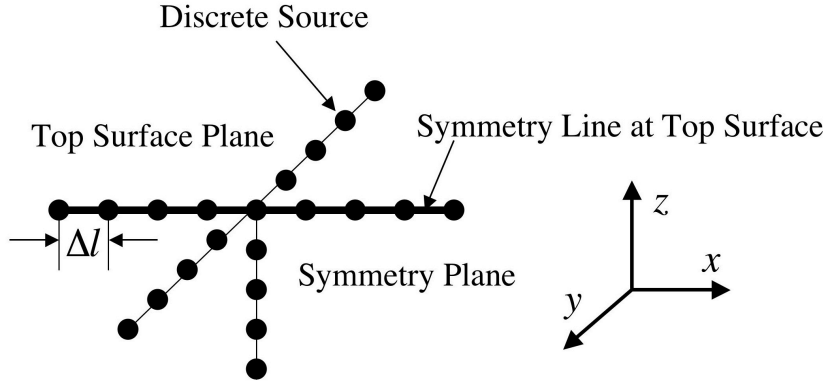
Figure 2. Experimentally measured transverse weld cross sections of solidification and transformation boundaries (WELD 1).
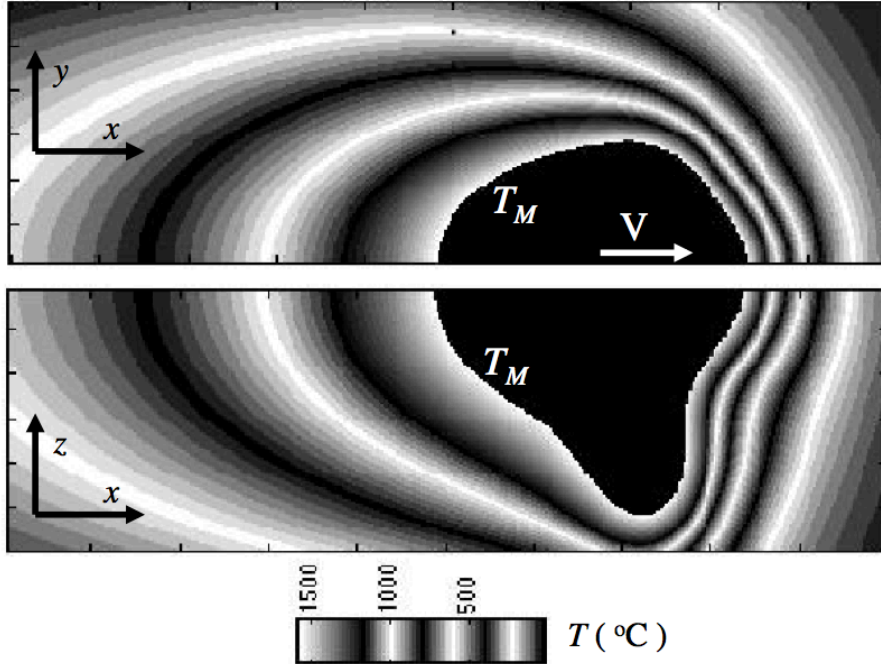

Figure 3. Two-dimensional slices, at half workpiece top surface and longitudinal cross section at symmetry plane, of three-dimensional temperature field (^{o}C) calculated using cross section information given in Table 1 for solidification boundary (WELD 1).
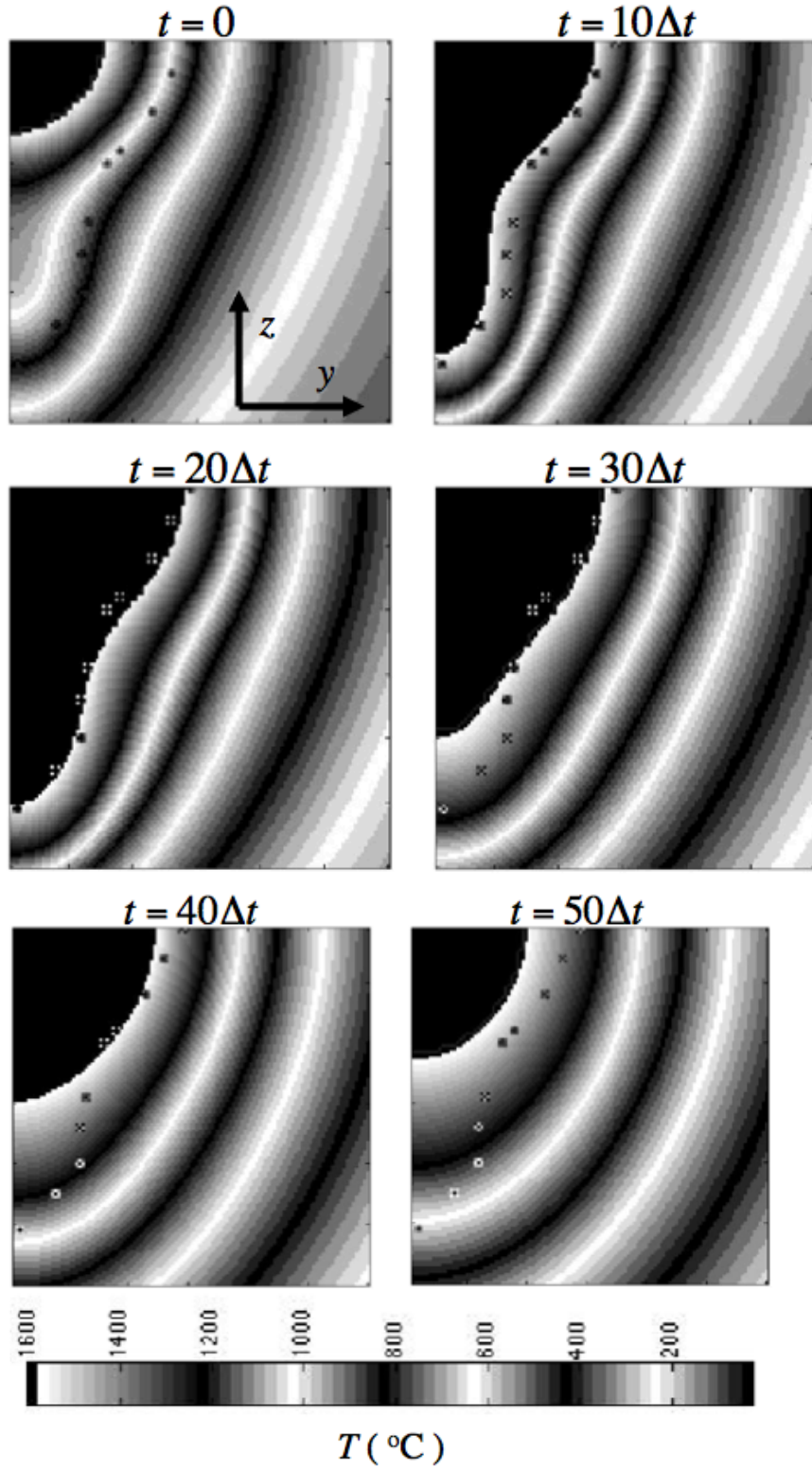
T (^{o}C)

9

Figure 4. Temperature history (°C) of transverse cross section of weld calculated using cross section information given in Table 1 for solidification boundary, where $\Delta t = \Delta l / V$, $\Delta l = (2.4/60)$ mm and $V = 16.9$ cm/s (WELD 1).
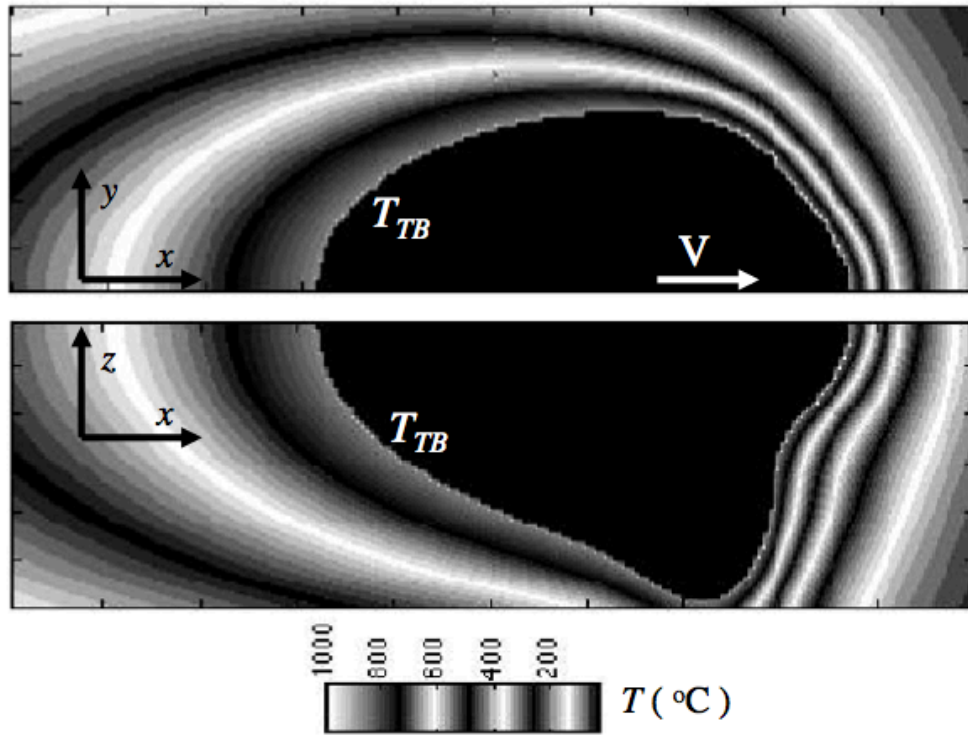
Figure 5. Two-dimensional slices, at half workpiece top surface and longitudinal cross section at symmetry plane, of three-dimensional temperature field ($^{\circ}$C) calculated using cross section information given in Table 2 for the transformation boundary (WELD 1).
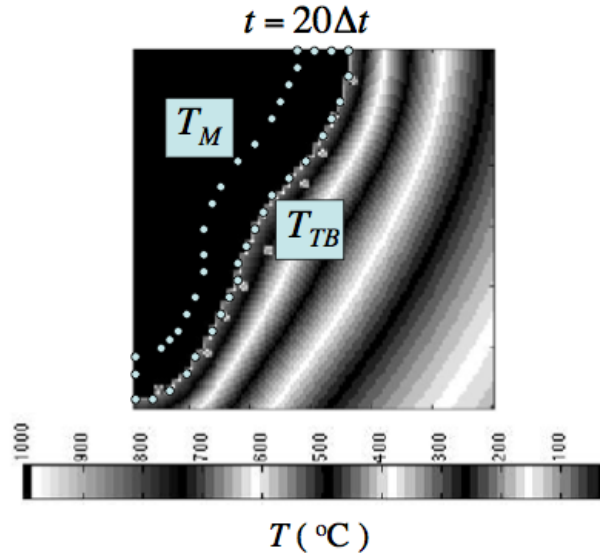

Figure 6. Temperature field ($^{\circ}$C) of transverse cross section of weld at given time calculated using cross section information given in Tables 1 and 2 for solidification and transformation boundaries, respectively, where $\Delta t = \Delta l / V$, $\Delta l = (2.4/60)$ mm and V = 16.9 cm/s (WELD 1).
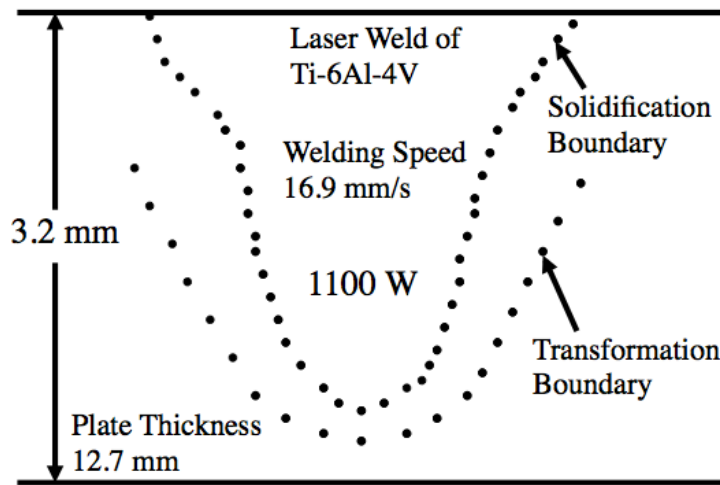
11

Figure 7. Experimentally measured transverse weld cross sections of solidification and transformation boundaries (WELD 2).
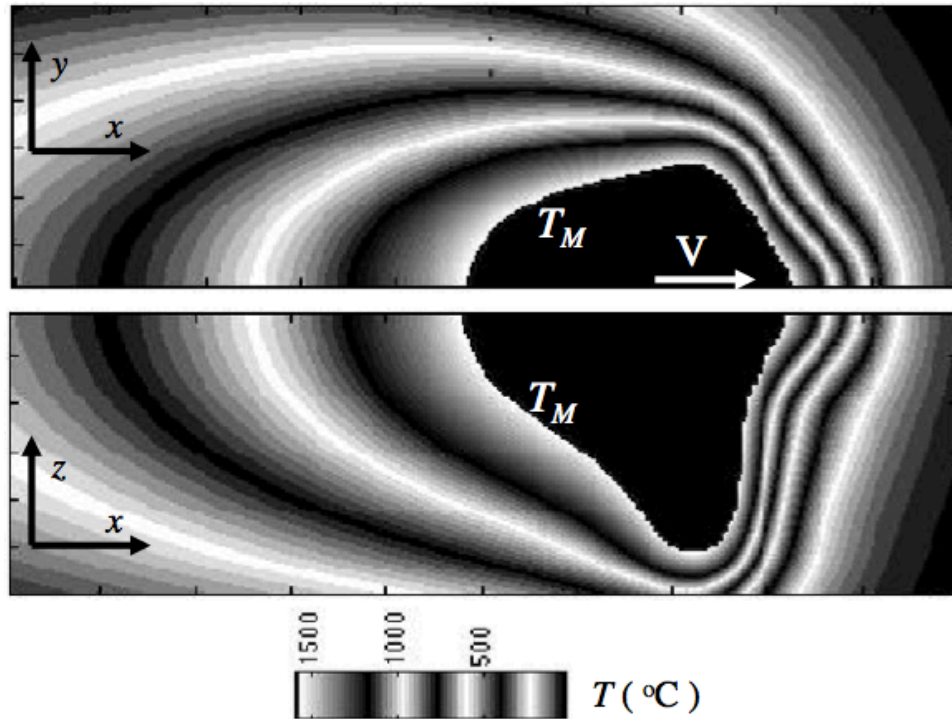

Figure 8. Two-dimensional slices, at half workpiece top surface and longitudinal cross section at symmetry plane, of three-dimensional temperature field ($^\circ$C) calculated using cross section information given in Table 1 for solidification boundary (WELD 2).
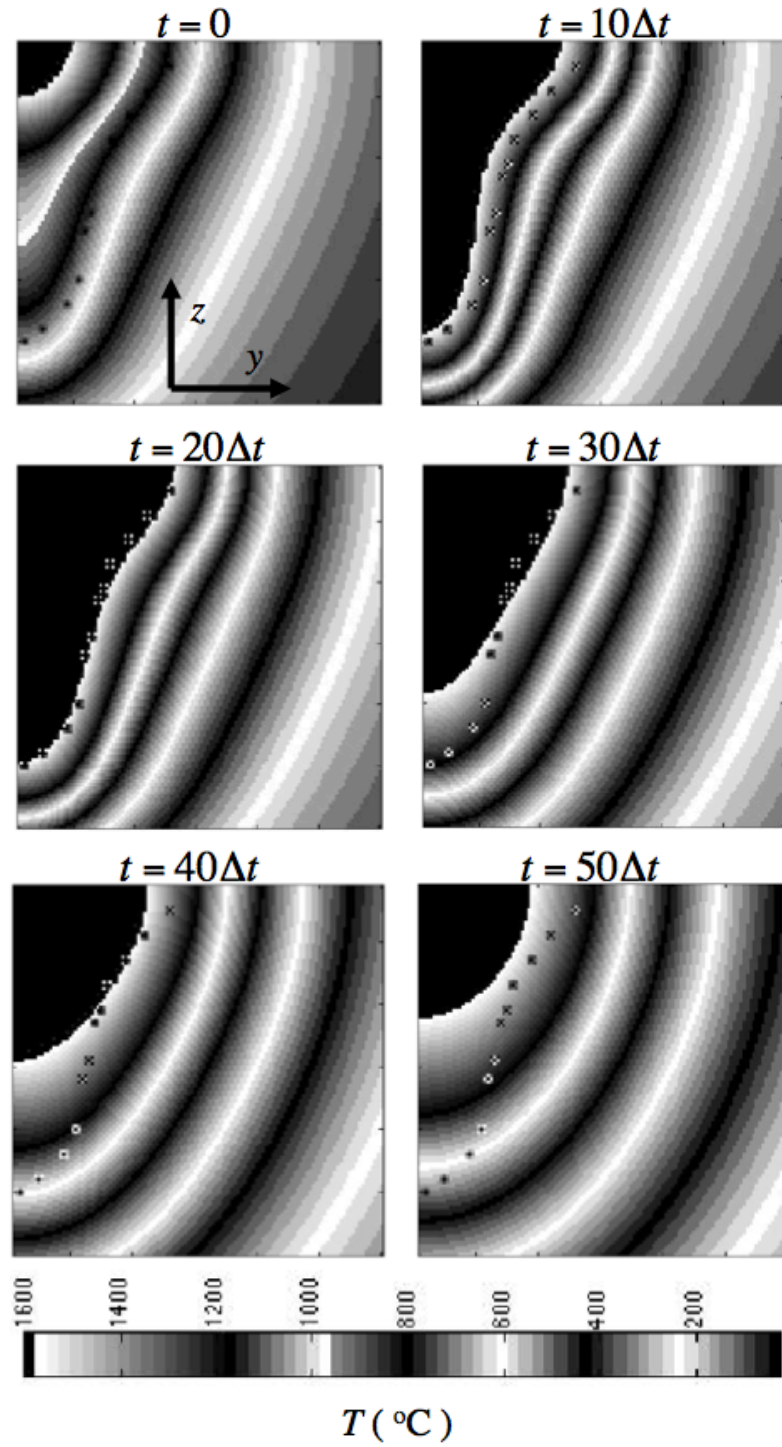
Figure 9. Temperature history (^{o}C) of transverse cross section of weld calculated using cross section information given in Table 1 for solidification boundary, where $\Delta t = \Delta l / V$, $\Delta l = (3.2/60)$ mm and $V = 16.9$ cm/s (WELD 2).
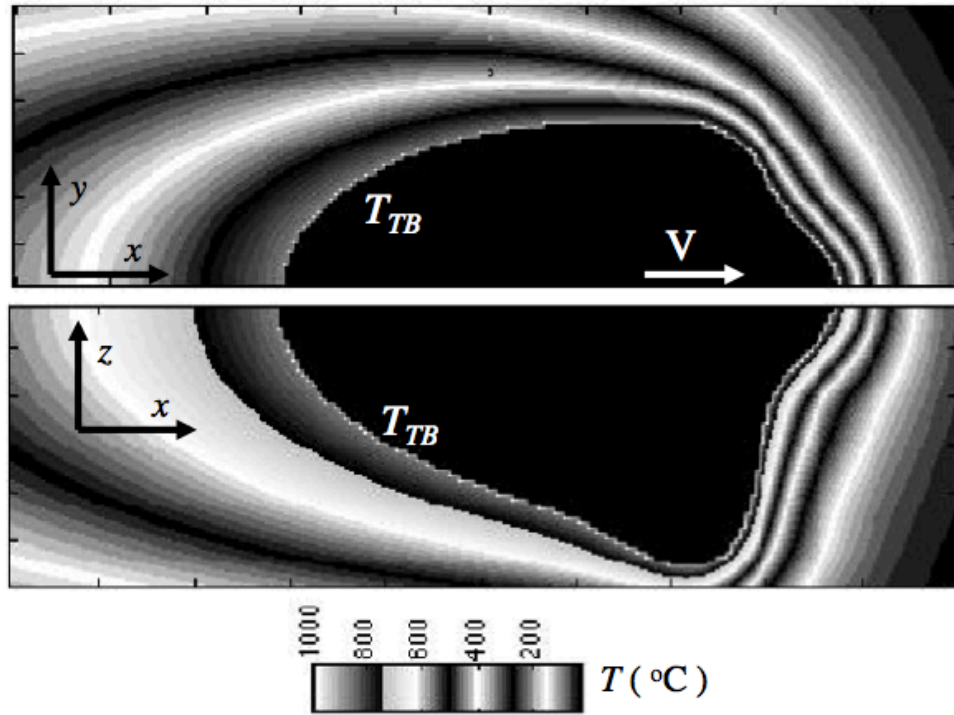
13

Figure 10. Two-dimensional slices, at half workpiece top surface and longitudinal cross section at symmetry plane, of three-dimensional temperature field (^{o}C) calculated using cross section information given in Table 2 for the transformation boundary (WELD 2).

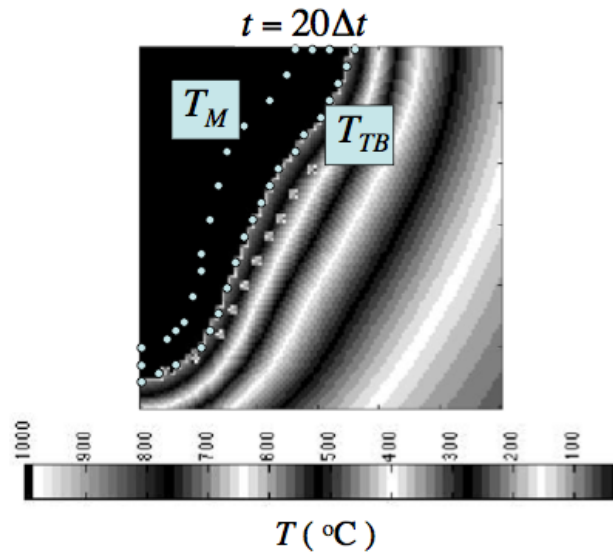**Figure 11.** Temperature field (^{o}C) of transverse cross section of weld at given time calculated using cross section information given in Tables 1 and 2 for solidification and transformation boundaries, respectively, where $\Delta t = \Delta l / V$, $\Delta l = (3.2/60)$ mm and V = 16.9 cm/s (WELD 2).

14

Figure 12. Experimentally measured transverse weld cross sections of solidification and transformation boundaries (WELD 3).
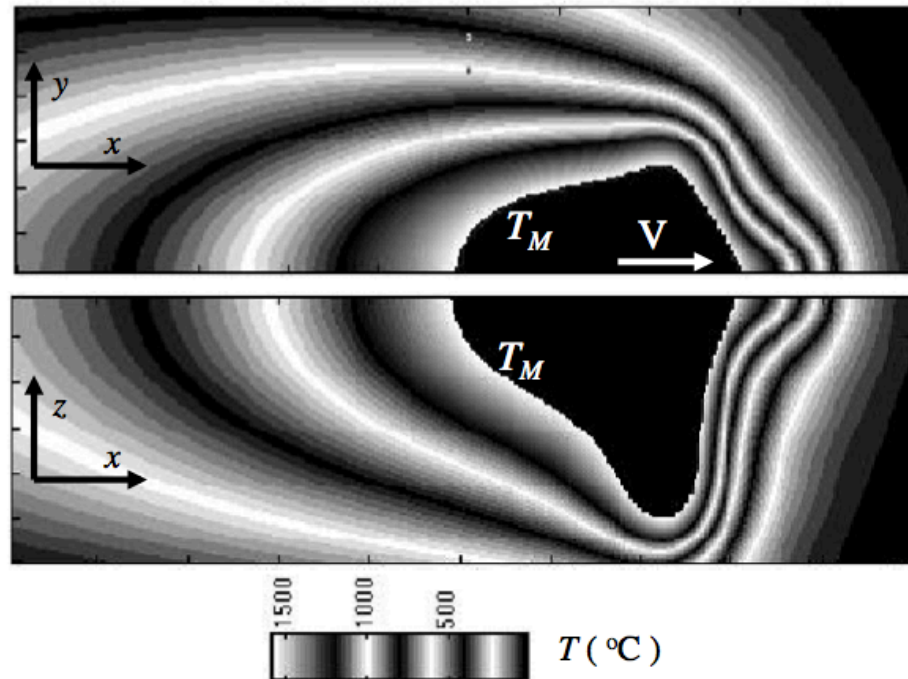
Figure 13. Two-dimensional slices, at half workpiece top surface and longitudinal cross section at symmetry plane, of three-dimensional temperature field (^{o}C) calculated using cross section information given in Table 1 for solidification boundary (WELD 3).

Figure 14. Temperature history (°C) of transverse cross section of weld calculated using cross section information given in Table 1 for solidification boundary, where $\Delta t = \Delta l / V$, $\Delta l = (3.8/60)$ mm and $V = 16.9$ cm/s (WELD 3).

Figure 15. Two-dimensional slices, at half workpiece top surface and longitudinal cross section at symmetry plane, of three-dimensional temperature field (^{o}C) calculated using cross section information given in Table 2 for the transformation boundary (WELD 3).

Figure 16. Temperature field (^{o}C) of transverse cross section of weld at given time calculated using cross section information given in Tables 1 and 2 for solidification and transformation boundaries, respectively, where $\Delta t = \Delta l / V$, $\Delta l = (3.8/60)$ mm and $V = 16.9$ cm/s (WELD 3).
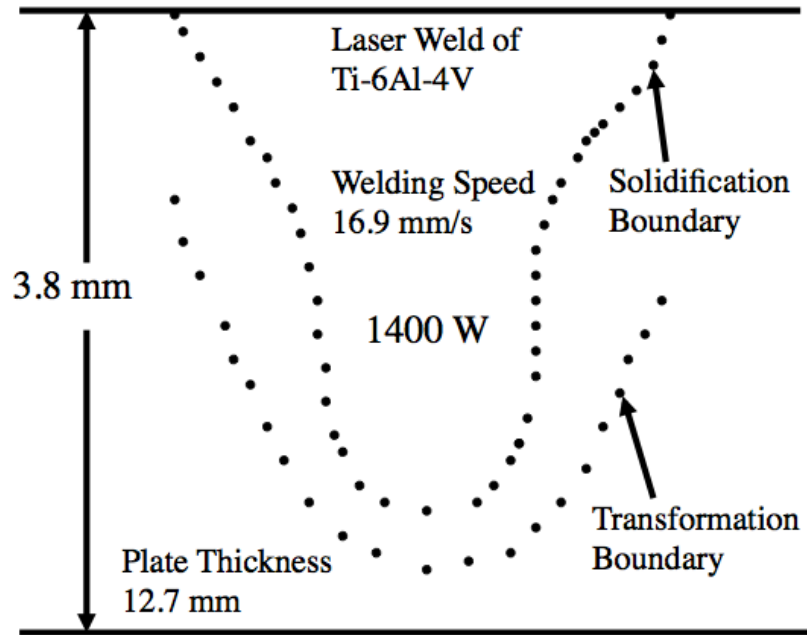
17

Figure 17. Experimentally measured transverse weld cross sections of solidification and transformation boundaries (WELD 4).

Figure 18. Two-dimensional slices, at half workpiece top surface and longitudinal cross section at symmetry plane, of three-dimensional temperature field ($^{\circ}$C) calculated using cross section information given in Table 1 for solidification boundary (WELD 4).

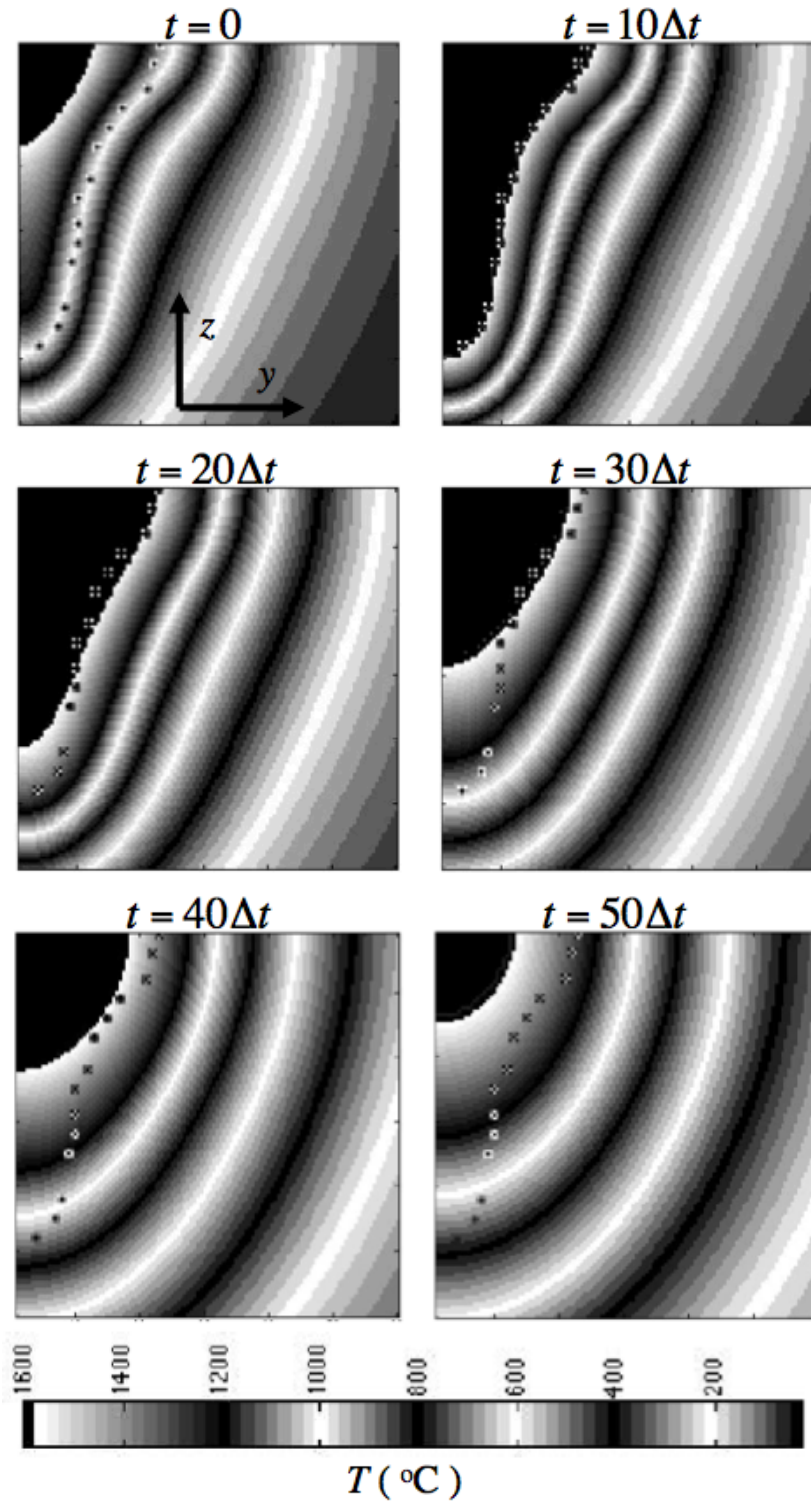**Figure 19.** Temperature history (°C) of transverse cross section of weld calculated using cross section information given in Table 1 for solidification boundary, where $\Delta t = \Delta l / V$, $\Delta l = (3.1/60)$ mm and V = 16.9 cm/s (WELD 4).
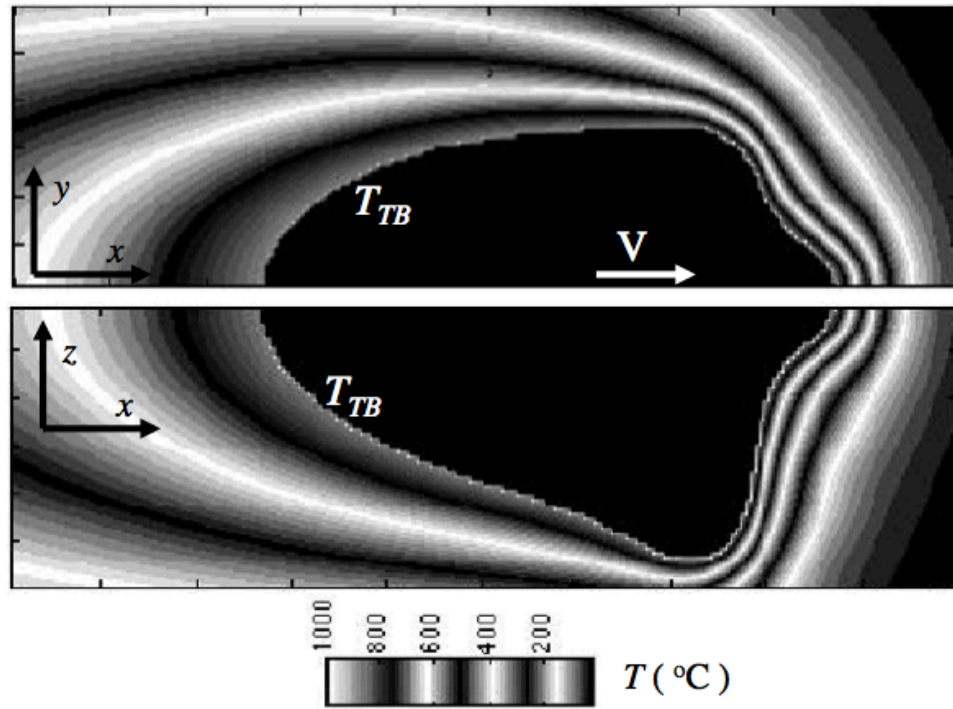

Figure 20. Two-dimensional slices, at half workpiece top surface and longitudinal cross section at symmetry plane, of three-dimensional temperature field (°C) calculated using cross section information given in Table 2 for the transformation boundary (WELD 4).

$t = 13\Delta t$
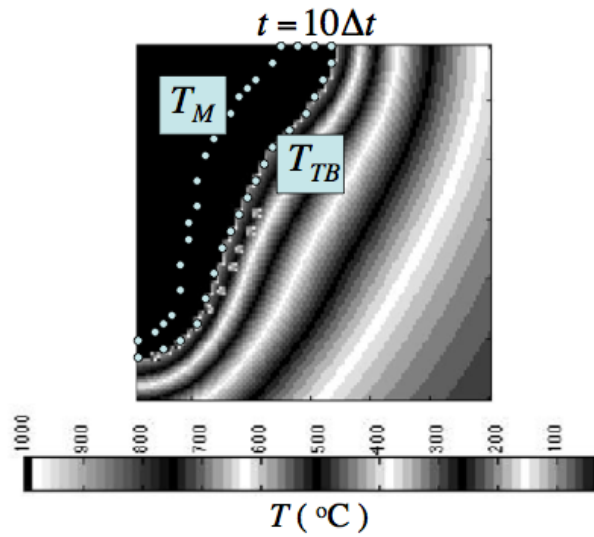
T_M

T_{TB}

$T(^oC)$

Figure 21. Temperature field (^{o}C) of transverse cross section of weld at given time calculated using cross section information given in Tables 1 and 2 for solidification and transformation boundaries, respectively, where $\Delta t = \Delta l /V$, $\Delta l = (3.1/60)$ mm and V = 16.9 cm/s (WELD 4).
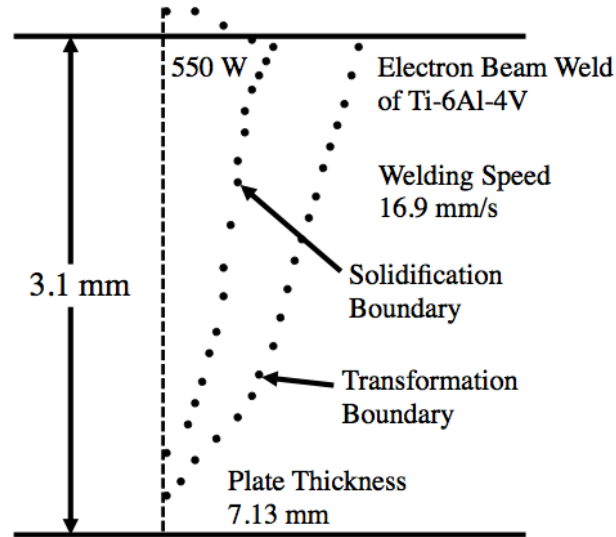

y

x

T_M

V

T_M

z

x

$T(^oC)$
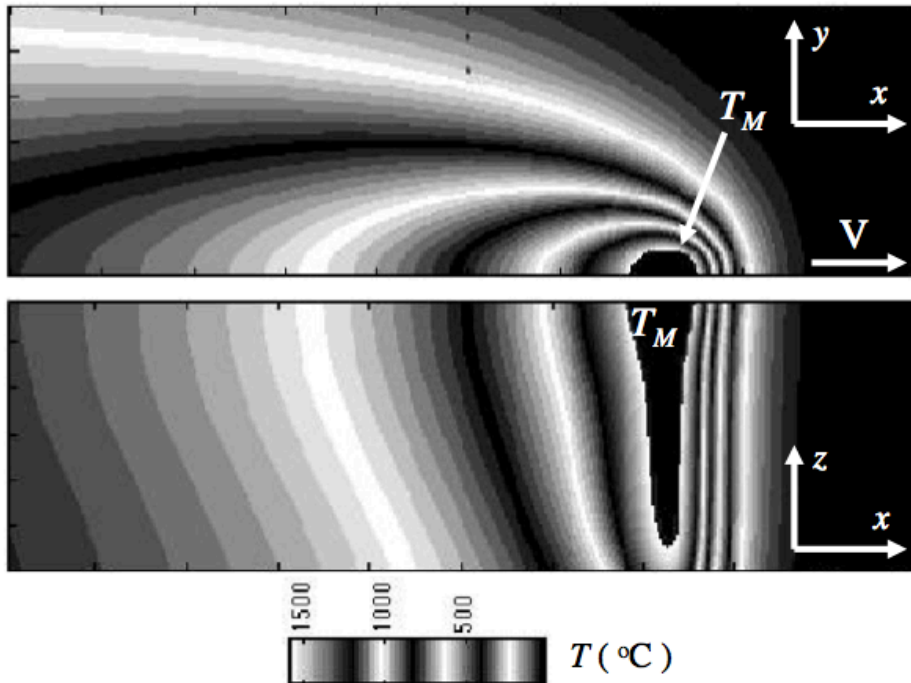
Figure 22. Experimentally measured transverse weld cross sections of solidification and transformation boundaries (WELD 5).

1114 W

6.0 mm

Electron Beam Weld of Ti-6Al-4V

Welding Speed 16.9 mm/s

Solidification Boundary

Transformation Boundary
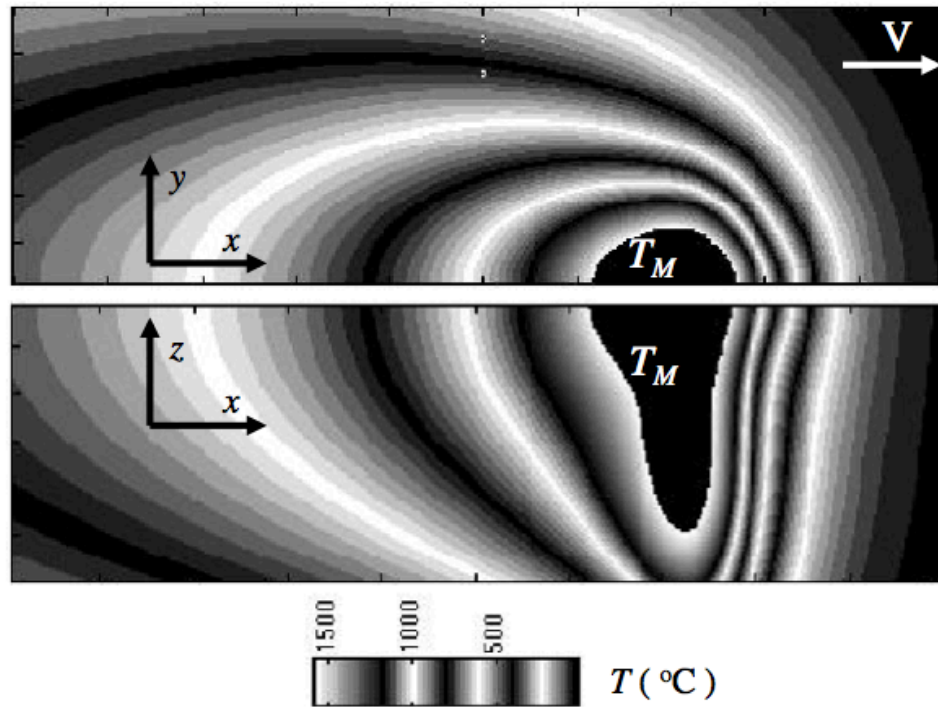
Plate Thickness 7.13 mm

Figure 23. Two-dimensional slices, at half workpiece top surface and longitudinal cross section at symmetry plane, of three-dimensional temperature field (^{o}C) calculated using cross section information given in Table 1 for solidification boundary (WELD 5).
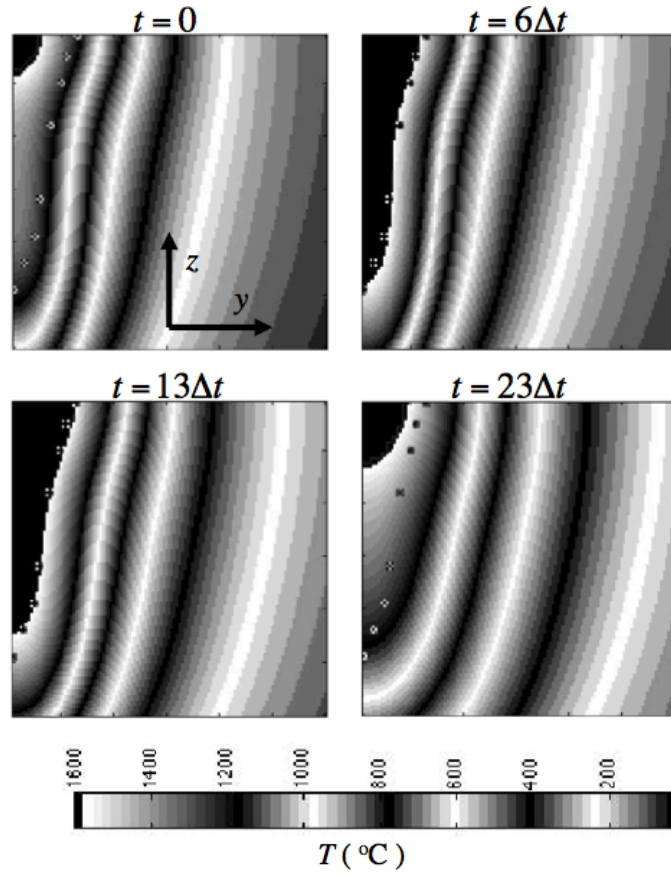
20
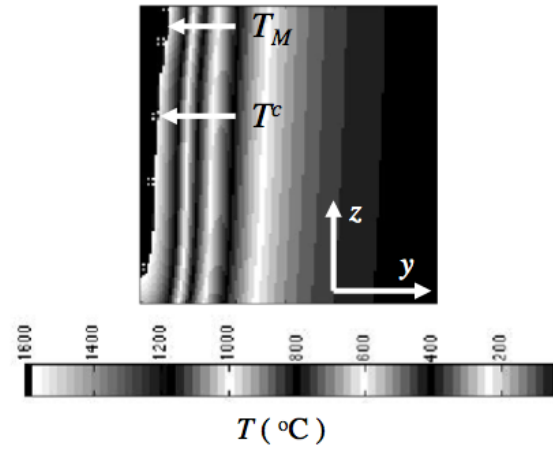
Figure 24. Temperature field (°C) of transverse cross section of weld at a given time calculated using cross section information given in Table 1 for solidification boundary, where $\Delta t = \Delta l /V$, $\Delta l = (6.0/60)$ mm and V = 16.9 cm/s (WELD 5).
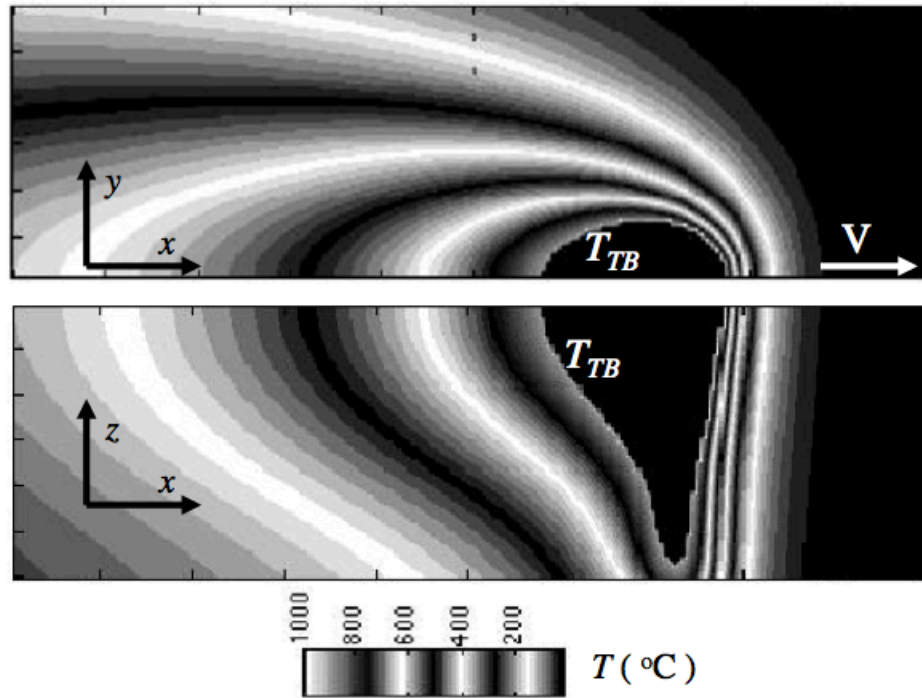
Figure 25. Two-dimensional slices, at half workpiece top surface and longitudinal cross section at symmetry plane, of three-dimensional temperature field (°C) calculated using cross section information given in Table 2 for the transformation boundary (WELD 5).

21
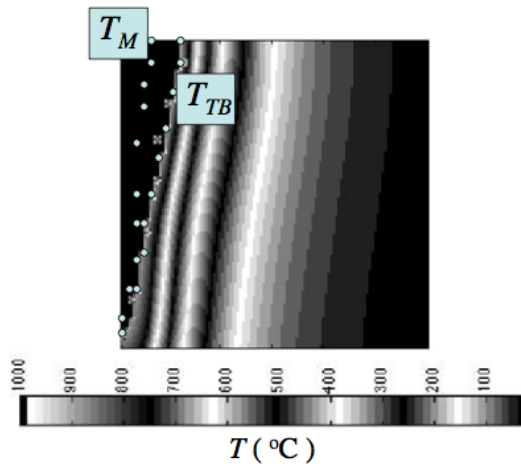
Figure 26. Temperature field (°C) of transverse cross section of weld at given time calculated using cross section information given in Tables 1 and 2 for solidification and transformation boundaries, respectively, where $\Delta t = \Delta l / V$, $\Delta l = (6.0/60)$ mm and $V = 16.9$ cm/s (WELD 5).
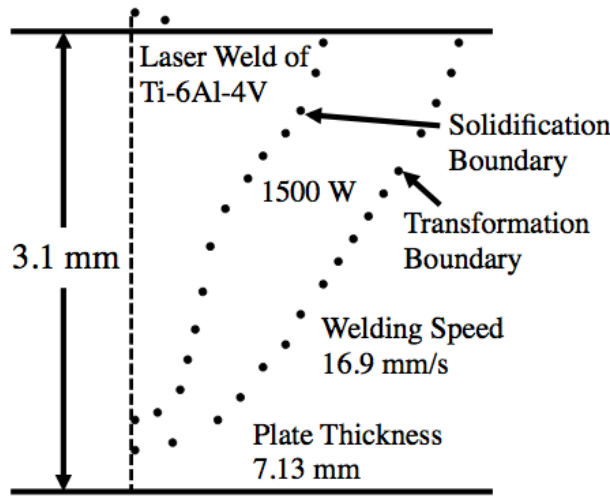
Figure 27. Experimentally measured transverse weld cross sections of solidification and transformation boundaries (WELD 6).
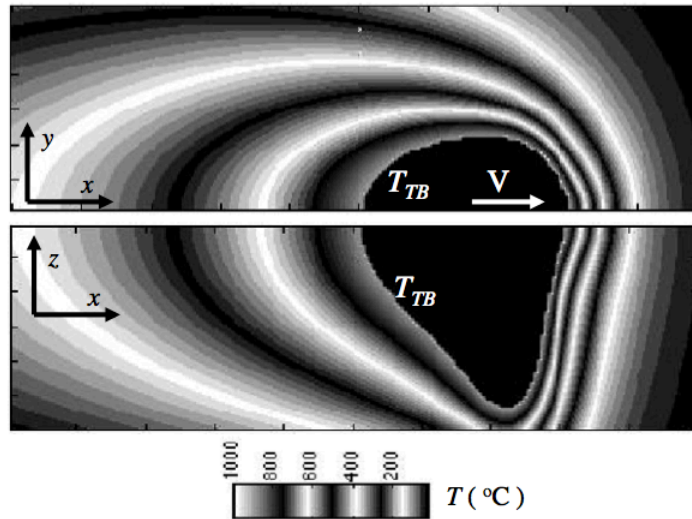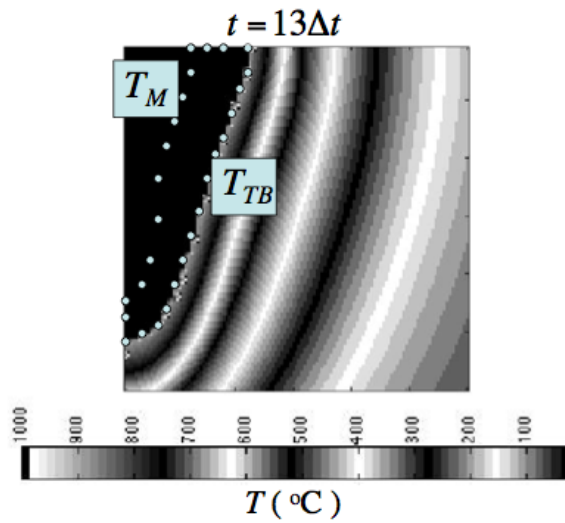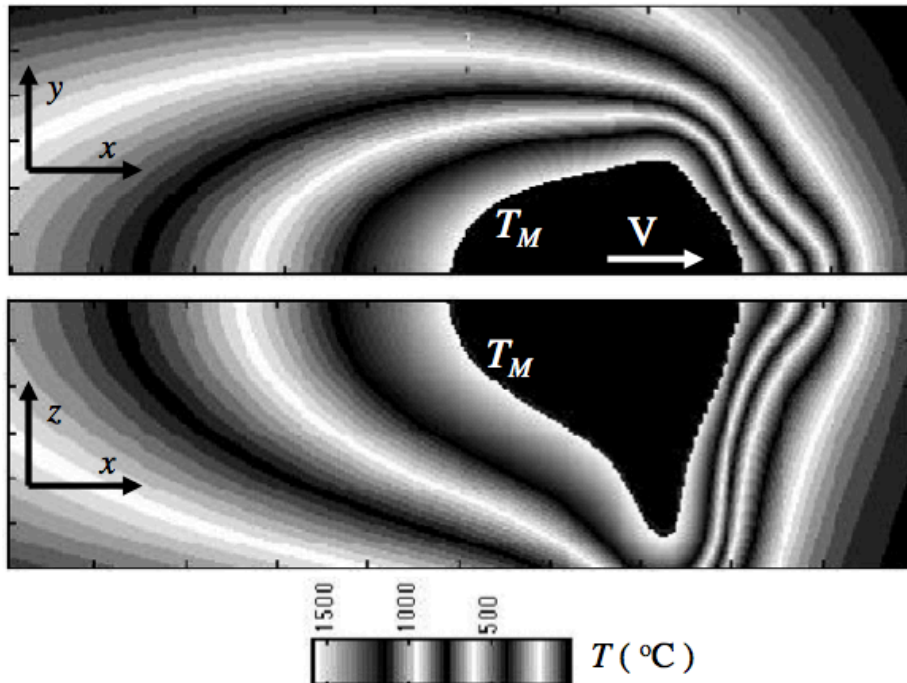

Figure 28. Two-dimensional slices, at half workpiece top surface and longitudinal cross section at symmetry plane, of three-dimensional temperature field (°C) calculated using cross section information given in Table 1 for solidification boundary (WELD 6).

Figure 29. Temperature history (^{o}C) of transverse cross section of weld calculated using cross section information given in Table 1 for solidification boundary, where $\Delta t = \Delta t /V$, $\Delta t = (3.1/60)$ mm and V = 16.9 cm/s (WELD 6).
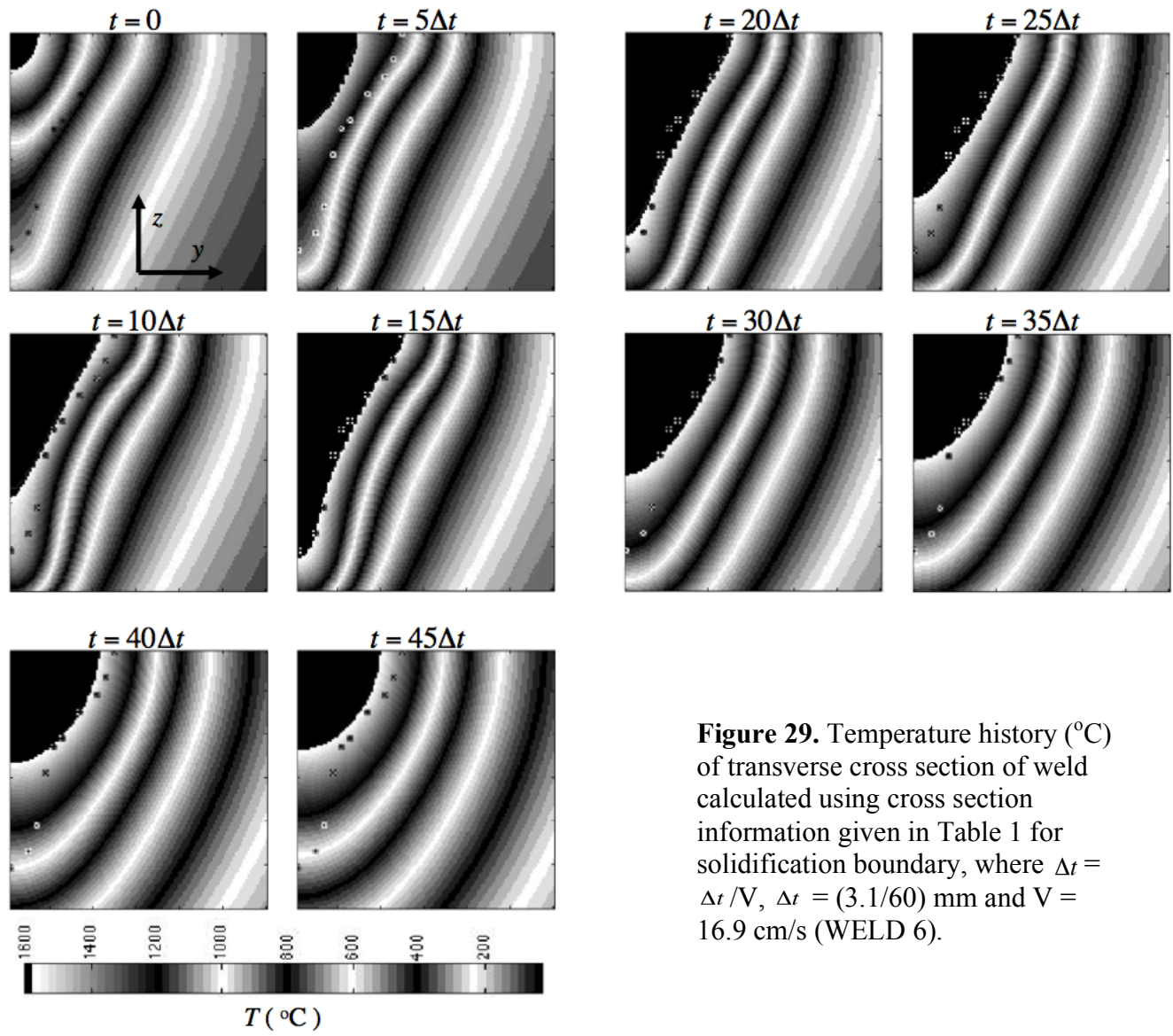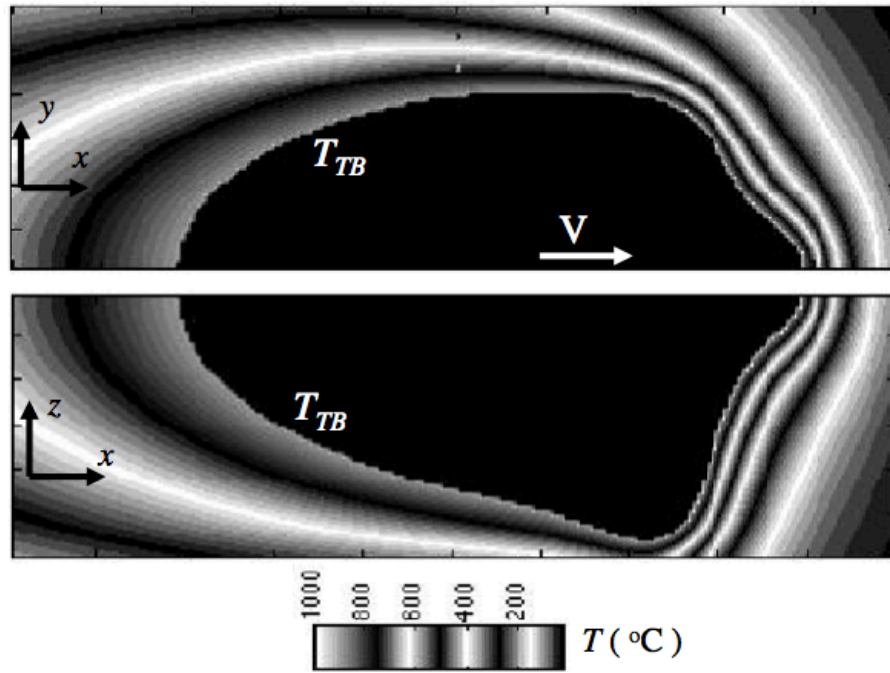
Figure 30. Two-dimensional slices, at half workpiece top surface and longitudinal cross section at symmetry plane, of three-dimensional temperature field ($^{\circ}$C) calculated using cross section information given in Table 2 for the transformation boundary (WELD 6).
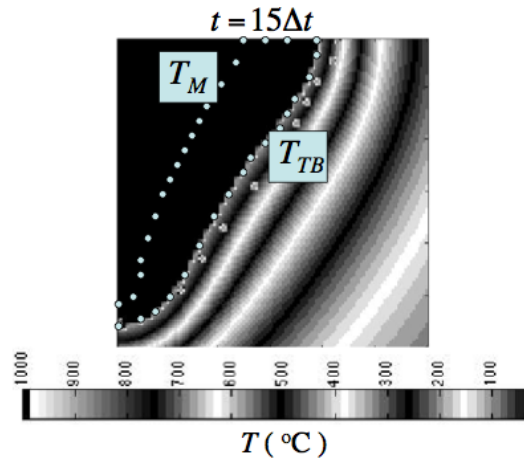
Figure 31. Temperature field ($^{\circ}$C) of transverse cross section of weld at given time calculated using cross section information given in Tables 1 and 2 for solidification and transformation boundaries, respectively, where $\Delta t = \Delta t / V$, $\Delta t = (3.1/60)$ mm and $V = 16.9$ cm/s (WELD 6).
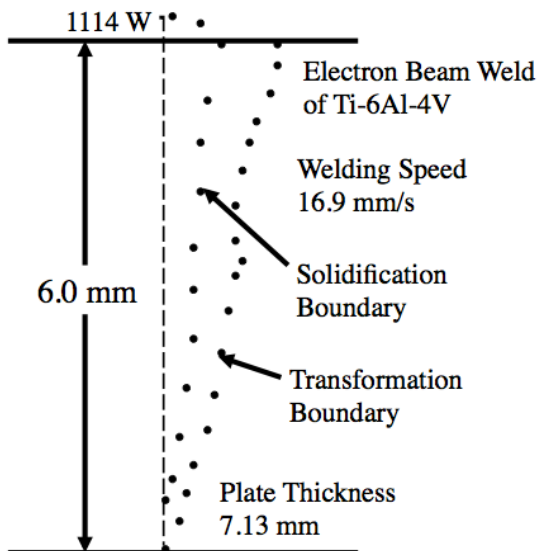
Table 1 Temperature field constraint conditions at positions (y_c, z_c) at solidification boundaries on transverse cross sections of Ti-6Al-4V welds

WELD 1 (720 W)	WELD 2 (1100 W)	WELD 3 (1400 W)
$(y_c$ mm, z_c mm)	$(y_c$ mm, z_c mm)	$(y_c$ mm, z_c mm)
(1.172, 0.0558)	(1.393, 0.3096)	(1.489, 0.103)
(1.060, 0.279)	(1.187, 0.516)	(1.438, 0.308)
(0.949, 0.5022)	(1.032, 0.722)	(1.335, 0.514)
(0.725, 0.725)	(0.877, 0.929)	(1.130, 0.719)
(0.670, 0.837)	(0.826, 1.135)	(0.976, 0.924)
(0.558, 1.172)	(0.774, 1.238)	(0.873, 1.130)
(0.502, 1.395)	(0.722, 1.548)	(0.770, 1.440)
(0.502, 1.620)	(0.671, 1.754)	(0.668, 1.644)
(0.335, 1.840)	(0.619, 2.167)	(0.668, 1.850)
(0.112, 2.065)	(0.516, 2.374)	(0.668, 2.055)
	(0.310, 2.580)	(0.616, 2.260)
	(0.155, 2.683)	(0.565, 2.671)
		(0.462, 2.876)
		(0.257, 3.080)

WELD 4 (550 W)	WELD 5 (1114 W)	WELD 6 (1500 W)
$(y_c$ mm, z_c mm)	$(y_c$ mm, z_c mm)	$(y_c$ mm, z_c mm)
(0.7086, 0.0886)	(0.667, 0.1667)	(1.321, 0.1016)
(0.620, 0.2657)	(0.500, 0.833)	(1.219, 0.4064)
(0.531, 0.531)	(0.467, 2.333)	(1.118, 0.6096)
(0.443, 0.974)	(0.3333, 3.667)	(0.9144, 0.8128)
(0.3543, 1.683)	(0.0833, 5.333)	(0.7112, 1.118)
(0.2657, 2.037)		(0.6096, 1.219)
(0.1771, 2.303)		(0.508, 1.524)
(0.0886, 2.569)		(0.4064, 2.134)
		(0.3048, 2.439)
		(0.1016, 2.642)

Table 2 Temperature field constraint conditions at positions (y_c, z_c) at transformation boundaries on transverse cross sections of Ti-6Al-4V welds

WELD 1 (720 W)	WELD 2 (1100 W)	WELD 3 (1400 W)
$(y_c$ mm, z_c mm)	$(y_c$ mm, z_c mm)	$(y_c$ mm, z_c mm)
(1.507, 0.279)	(1.548, 1.135)	(1.386, 1.850)
(1.395, 0.502)	(1.393, 1.342)	(1.284, 2.055)
(1.283, 0.7254)	(1.290, 1.548)	(1.181, 2.260)
(1.172, 0.9486)	(1.187, 1.754)	(1.080, 2.465)
(0.949, 1.395)	(1.084, 1.960)	(0.976, 2.671)
(0.780, 1.620)	(0.980, 2.167)	(0.873, 2.876)
(0.670, 1.840)	(0.877, 2.374)	(0.719, 3.080)
(0.558, 2.065)	(0.774, 2.580)	(0.514, 3.285)
(0.223, 2.288)	(0.568, 2.786)	(0.308, 3.388)
	(0.310, 2.890)	

Table 2 (continued)

WELD 4 (550 W)	WELD 5 (1114 W)	WELD 6 (1500 W)
(y_c mm, z_c mm)	*(y_c mm, z_c mm)*	*(y_c mm, z_c mm)*
(1.240, 0.886)	(1.333, 0.500)	(2.235, 0.1016)
(1.151, 0.3543)	(1.000, 1.333)	(2.184, 0.3048)
(1.063,0.620)	(0.8333, 2.00)	(2.032, 0.508)
(0.974,0.8857)	(0.8333, 2.833)	(1.930, 0.7112)
(0.8857, 1.240)	(0.667, 3.833)	(1.829, 0.9144)
(0.797, 1.417)	(0.333, 5.167)	(1.626, 1.219)
(0.7086, 1.771)	(0.1667, 5.833)	(1.422, 1.524)
(0.620, 2.126)		(1.118, 1.930)
(0.531, 2.303)		(0.9144, 2.235)
(0.4333, 2.480)		(0.7112, 2.540)
(0.0886, 2.834)		(0.1016,2.845)

Table 3 Volumetric source function $C(\hat{x}_k)$ calculated according to solidification-boundary constraint conditions given in Table 1 for input power of 720 W, where Δt = (2.4/60) mm (WELD 1), and $x_k = y_k = 0$ for k = 1 to 12.

k	$C_k/0.9$	z_k (Δt)
1	0.031	1
2	0.013	5
3	0.011	10
4	0.011	15
5	0.011	20
6	0.011	25
7	0.015	30
8	0.023	35
9	0.033	40
10	0.033	45
11	0.033	50
12	0.022	55

k	C_k	x_k (Δt)	y_k (Δt)	z_k (Δt)
13	0.033	-15.0	0.0	1
14	0.008	-25.0	0.0	1
15	0.033	15.0	0.0	1
16	0.008	25.0	0.0	1
17	0.033	0.0	-15.0	1
18	0.008	0.0	-25.0	1
19	0.033	0.0	15.0	1
20	0.008	0.0	25.0	1

Table 4 Volumetric source function $C(\hat{x}_k)$ calculated according to solidification-boundary constraint conditions given in Table 1 for input power of 1100 W, where $\Delta t = (3.2/60)$ mm (WELD 2) and $x_k = y_k = 0$ for $k = 1$ to 12.

k	$C_k/1.6$	z_k (Δt)
1	0.031	1
2	0.020	5
3	0.019	10
4	0.017	15
5	0.017	20
6	0.025	25
7	0.029	30
8	0.029	35
9	0.031	40
10	0.034	45
11	0.033	50
12	0.013	55

k	C_k	x_k (Δt)	y_k (Δt)	z_k (Δt)
13	0.033	-15.0	0.0	1
14	0.031	-25.0	0.0	1
15	0.033	15.0	0.0	1
16	0.031	25.0	0.0	1
17	0.033	0.0	-15.0	1
18	0.031	0.0	-25.0	1
19	0.033	0.0	15.0	1
20	0.031	0.0	25.0	1

Table 5 Volumetric source function $C(\hat{x}_k)$ calculated according to solidification-boundary constraint conditions given in Table 1 for input power of 1400 W, where $\Delta t = (3.8/60)$ mm (WELD 3) and $x_k = y_k = 0$ for $k = 1$ to 12.

k	$C_k/2.2$	z_k (Δt)
1	0.031	1
2	0.020	5
3	0.020	10
4	0.025	15
5	0.025	20
6	0.026	25
7	0.027	30
8	0.027	35
9	0.032	40
10	0.034	45
11	0.033	50
12	0.013	55

Table 5 (continued)

k	C_k	x_k (Δt)	y_k (Δt)	z_k (Δt)
13	0.033	-15.0	0.0	1
14	0.052	-25.0	0.0	1
15	0.033	15.0	0.0	1
16	0.052	25.0	0.0	1
17	0.033	0.0	-15.0	1
18	0.052	0.0	-25.0	1
19	0.033	0.0	15.0	1
20	0.052	0.0	25.0	1

Table 6 Volumetric source function $C(\hat{x}_k)$ calculated according to solidification-boundary constraint conditions given in Table 1 for input power of 550 W, where Δt = (3.1/60) mm (WELD 4) and $x_k = y_k = 0$ for $k = 1$ to 14.

k	$C_k/2.2$	z_k (Δt)
1	0.031	1
2	0.015	5
3	0.015	10
4	0.025	15
5	0.025	20
6	0.026	25
7	0.027	30
8	0.027	35
9	0.032	40
10	0.034	45
11	0.022	50
12	0.022	55
13	0.024	60
14	0.032	65

k	C_k	x_k (Δt)	y_k (Δt)	z_k (Δt)
15	0.030	-15.0	0.0	1
16	0.030	15.0	0.0	1
17	0.030	0.0	-15.0	1
18	0.030	0.0	15.0	1

Table 7 Volumetric source function $C(\hat{x}_k)$ calculated according to solidification-boundary constraint conditions given in Table 1 for input power of 1114 W, where $\Delta t = (6.0/60)$ mm (WELD 5) and $x_k = y_k = 0$ for $k = 1$ to 14.

k	$C_k/2.5$	z_k (Δt)
1	0.1	1
2	0.1	5
3	0.1	10
4	0.1	15
5	0.1	20
6	0.1	25
7	0.1	30
8	0.1	35
9	0.1	40
10	0.1	45
11	0.1	50
12	0.1	55
13	0.1	60
14	0.1	65

Table 8 Volumetric source function $C(\hat{x}_k)$ calculated according to solidification-boundary constraint conditions given in Table 1 for input power of 1500 W, where $\Delta t = (3.1/60)$ mm (WELD 6) and $x_k = y_k = 0$ for $k = 1$ to 13.

k	C_k	z_k (Δt)
1	0.1	1
2	0.1	5
3	0.1	10
4	0.1	15
5	0.055	20
6	0.05	25
7	0.05	30
8	0.048	35
9	0.048	40
10	0.05	45
11	0.062	50
12	0.085	55
13	0.083	60

k	C_k	x_k (Δt)	y_k (Δt)	z_k (Δt)
14	0.071	-25.0	0.0	1
16	0.071	25.0	0.0	1
17	0.071	0.0	-25.0	1
19	0.071	0.0	25.0	1

Table 9 Volumetric source function $C(\hat{x}_k)$ calculated according to transformation-boundary constraint conditions given in Table 2 for input power of 720 W, where $\Delta t = (2.4/60)$ mm (WELD 1) and $x_k = y_k = 0$ for $k = 1$ to 13.

k	$C_k/0.51$	z_k (Δt)
1	0.031	1
2	0.014	5
3	0.014	10
4	0.014	15
5	0.014	20
6	0.015	25
7	0.016	30
8	0.020	35
9	0.032	40
10	0.034	45
11	0.034	50
12	0.022	55
13	0.022	60

k	C_k	x_k (Δt)	y_k (Δt)	z_k (Δt)
14	0.033	-15.0	0.0	1
15	0.008	-25.0	0.0	1
16	0.033	15.0	0.0	1
17	0.008	25.0	0.0	1
18	0.033	0.0	-15.0	1
19	0.008	0.0	-25.0	1
20	0.033	0.0	15.0	1
21	0.008	0.0	25.0	1

Table 10 Volumetric source function $C(\hat{x}_k)$ calculated according to transformation-boundary constraint conditions given in Table 2 for input power of 1100 W, where $\Delta t = (3.2/60)$ mm (WELD 2) and $x_k = y_k = 0$ for $k = 1$ to 12.

k	$C_k/1.1$	z_k (Δt)
1	0.031	1
2	0.020	5
3	0.020	10
4	0.025	15
5	0.025	20
6	0.026	25
7	0.027	30
8	0.027	35
9	0.032	40
10	0.034	45
11	0.033	50
12	0.010	55

Table 10 (continued)

k	C_k	x_k (Δt)	y_k (Δt)	z_k (Δt)
13	0.033	-15.0	0.0	1
14	0.031	-25.0	0.0	1
15	0.033	15.0	0.0	1
16	0.031	25.0	0.0	1
17	0.033	0.0	-15.0	1
18	0.031	0.0	-25.0	1
19	0.033	0.0	15.0	1
20	0.031	0.0	25.0	1

Table 11 Volumetric source function $C(\hat{x}_k)$ calculated according to transformation-boundary constraint conditions given in Table 2 for input power of 1400 W, where Δt = (3.8/60) mm (WELD 3) and $x_k = y_k =0$ for $k = 1$ to 11.

k	$C_k/1.6$	z_k (Δt)
1	0.031	1
2	0.030	5
3	0.030	10
4	0.030	15
5	0.030	20
6	0.030	25
7	0.030	30
8	0.030	35
9	0.032	40
10	0.034	45
11	0.033	50

k	C_k	x_k (Δt)	y_k (Δt)	z_k (Δt)
13	0.033	-15.0	0.0	1
14	0.052	-25.0	0.0	1
15	0.033	15.0	0.0	1
16	0.052	25.0	0.0	1
17	0.033	0.0	-15.0	1
18	0.052	0.0	-25.0	1
19	0.033	0.0	15.0	1
20	0.052	0.0	25.0	1

Table 12 Volumetric source function $C(\hat{x}_k)$ calculated according to transformation-boundary constraint conditions given in Table 2 for input power of 550 W, where $\Delta t = (3.1/60)$ mm (WELD 4) and $x_k = y_k = 0$ for $k = 1$ to 14.

k	$C_k/1.4$	z_k (Δt)
1	0.032	1
2	0.031	5
3	0.031	10
4	0.031	15
5	0.031	20
6	0.031	25
7	0.031	30
8	0.031	35
9	0.032	40
10	0.034	45
11	0.022	50
12	0.022	55
13	0.015	60
14	0.015	65

k	C_k	x_k (Δt)	y_k (Δt)	z_k (Δt)
15	0.030	-15.0	0.0	1
16	0.030	15.0	0.0	1
17	0.030	0.0	-15.0	1
18	0.030	0.0	15.0	1

Table 13 Volumetric source function $C(\hat{x}_k)$ calculated according to transformation-boundary constraint conditions given in Table 2 for input power of 1114 W, where $\Delta t = (6.0/60)$ mm (WELD 5) and $x_k = y_k = 0$ for $k = 1$ to 14.

k	$C_k/1.4$	z_k (Δt)
1	0.2	1
2	0.2	5
3	0.15	10
4	0.15	15
5	0.15	20
6	0.15	25
7	0.1	30
8	0.1	35
9	0.1	40
10	0.1	45
11	0.1	50
12	0.1	55
13	0.1	60
14	0.1	65

Table 14 Volumetric source function $C(\hat{x}_k)$ calculated according to transformation-boundary constraint conditions given in Table 2 for input power of 1500 W, where $\Delta t = (3.1/60)$ mm (WELD 6) and $x_k = y_k = 0$ for $k = 1$ to 12.

k	C_k	z_k (Δt)
1	0.1	1
2	0.1	5
3	0.1	10
4	0.1	15
5	0.055	20
6	0.05	25
7	0.05	30
8	0.048	35
9	0.048	40
10	0.05	45
11	0.062	50
12	0.027	55

k	C_k	x_k (Δt)	y_k (Δt)	z_k (Δt)
13	0.1	-25.0	0.0	1
14	0.1	25.0	0.0	1
15	0.1	0.0	-25.0	1
16	0.1	0.0	25.0	1